Erschienen in: Polymer Chemistry ; 5 (2014), 12. - S. 3771-3776
https://doi.org/10.1039/C4PY00263F

Geomimetics for green polymer synthesis: highly ordered polyimides *via* hydrothermal techniques†

Bettina Baumgartner,[a] Michael J. Bojdys[b] and Miriam M. Unterlass*[a]

Inspired by geological ore formation processes, we apply one-step hydrothermal (HT) polymerization to the toughest existing high-performance polymer, poly(*p*-phenyl pyromellitimide) (PPPI). We obtain highly-ordered and fully imidized PPPI as crystalline flakes and flowers on the micrometer scale. In contrast to classical 2-step procedures that require long reaction times and toxic solvents and catalysts, HT polymerization allows for full conversion in only 1 h at 200 °C, in nothing but hot water. Investigation of the crystal growth mechanism *via* scanning electron microscopy (SEM) suggests that PPPI aggregates form *via* a dissolution polymerization crystallization process, which is uniquely facilitated by the reaction conditions in the HT regime. A conventionally prefabricated polyimide did not recrystallize hydrothermally, indicating that the HT polymerization and crystallization occur simultaneously. The obtained material shows excellent crystallinity and remarkable thermal stability (600 °C under N_2) that stem from a combination of a strong, covalent polymer backbone and interchain hydrogen bonding.

1 Introduction

Polymers of high molecular weight are usually more difficult to crystallize than small molecules, and in most cases they are obtained as amorphous products. For high-performance polymers (HPPs), crystallinity is a desired feature: it enhances mechanical and thermal strength,[1] or directional properties such as electrical conductivity.[2] Whereas polymers of sufficient molecular flexibility may still be recrystallized from solution or the melt, this is not possible for HPPs as they are usually insoluble and infusible. Yaghi *et al.* established two paradigms of dynamic covalent chemistry for the synthesis of monolithic, high molecular weight, yet crystalline metal–organic frameworks (MOFs)[3] and covalent organic frameworks (COFs):[4,5] Firstly, the backbone of the structure needs to be sufficiently rigid (*i.e.* monomers should only link-up *via* bonds with low degrees of freedom). Second, the linking-chemistry needs to be sufficiently reversible to allow the formation of a thermodynamic, ordered product. Polyimides (PIs) are a class of HPPs where the building-blocks comprise usually aromatic moieties linked by strong covalent bonds, *i.e.* a cyclic imide. The formation of the cyclic imide is essentially irreversible. Since fully aromatic PIs are neither fusible nor soluble and do not provide dynamic covalent bonds, the formation of a thermodynamic, highly crystalline product is hard to conceive and challenging by traditional means. Our approach for the realization of a crystalline one-dimensional (1D) PI is inspired by nature. We apply geomimicry, *i.e.* the imitation of principles and conditions of geological systems in the laboratory. The earth's crust is the origin of various highly crystalline minerals. Such ores form, for example, in so-called hydrothermal (HT) crystallization processes that take place in hydrothermal veins, *i.e.* streams of coalesced water molecules at elevated temperatures and pressures (>100 °C and >1 bar).[6,7] These conditions can be mimicked in the laboratory using steel-autoclaves (ESI†). This approach is commonly used in inorganic synthesis of highly crystalline materials, *e.g.* gemstones or zeolites.[8,9] In organic synthesis, HT conditions have been proven highly fruitful for obtaining carbonaceous materials, which are however typically amorphous.[10,11] The target 1D polymer of this work is the fully aromatic polyimide (*aka* "arimid") poly(*p*-phenylene pyromellitimide) (PPPI, **5** in Scheme 1). PPPI is certainly the most challenging member of the polyimide (PI) family in terms of synthesis and processability. It is the most rigid PI,[12] with a predicted Young's modulus of over 500 GPa,[13] which is in the range of pure metals such as osmium, the highest value for a polymer ever reported.[14] Traditionally, PPPI is synthesized *via* detours: the monomers *p*-phenylendiamine (*p*-PDA, **1**, Scheme 1) and pyromellitic acid dianhydride (PMDA, **2**) are transformed into polymeric intermediates, poly(amic acids) (PAAs, **4**). In a second thermal annealing step, they are then reacted to the final PI by applying temperatures >500 °C (see Scheme 1). The resulting polymeric product is however semicrystalline at its best.

[a]*Technische Universitat Wien, Institute of Materials Chemistry, Department of Applied Inorganic Synthesis, Getreidemarkt 9/BC/2, A 1060 Vienna, Austria. E mail: miriam.unterlass@tuwien.ac.at*

[b]*Technische Universitat Berlin, Institute of Chemistry: Functional Materials, Hardenbergstr. 40, D 10623 Berlin, Germany*

† Electronic supplementary information (ESI) available: Experimental details, product aspect photographs, TGA, FT IR ATR, NMR, solubility tests, SEM, PXRD, and crystal structure data.

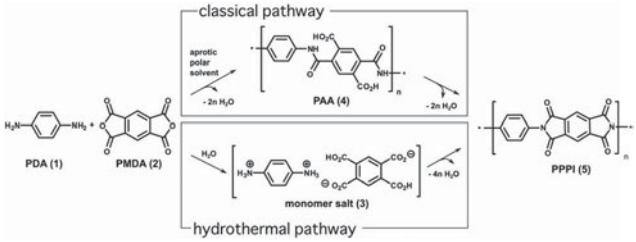

Scheme 1 HT *vs.* classical PPPI synthesis. PPPI (**5**) obtained from PDA (**1**) and PMDA (**2**). Classically, **1** and **2** are transformed into poly(amic acid) (PAA, **4**) intermediates prior to condensation to **5**. Hydrothermally, **1** and **2** react to the salt **3** *via* acid base-reaction before condensation to **5**.

In order to increase the crystallinity of PPPI Kimura *et al.* have presented an alternative process, using phase separation techniques, which however requires high-temperatures (>300 °C) and long reaction times (min 6 h).[12,15] Previous attempts to obtain polyimides hydrothermally did not achieve the target of high crystallinity.[16,17]

In this contribution, we introduce a simultaneous polymerization and crystallization approach, which gives direct access to the thermodynamically favored, highly crystalline product. Our approach yields PPPI, a 1D high-performance polymer, of impressive crystallinity that cannot be achieved by classical procedures. Intriguingly, hydrothermal synthesis of HPPs is inherently green: While the classical procedures rely on harsh synthetic environments, long reaction times, toxic solvents and catalysts, HT synthesis uses only water and yields full conversion after only 1 h.

2 Results and discussion

In our approach, hot water is used as the only reaction medium. When subjecting **1** and **2** to water, PMDA first hydrolyzes to pyromellitic acid (PMA) and the monomer salt $[(H_2PDA^{2+})(PMA^{2-})]$ (**3**) forms subsequently by acid–base reaction, as a consequence of the pK_A difference between amine and carboxylic acid functions and mediated by the protic solvent water. Since monomer salts have been shown to form as inevitable intermediates in HT polycondensation of polyimides,[17] we chose to start directly from compound **3**. Although separately **1** and **2** are highly soluble in water, upon mixing, **3** precipitates immediately as white polycrystalline powder, illustrating the high supersaturation at which it forms (ESI†). A dispersion of **3** in water is then filled into a glass liner and transferred to an autoclave. The autoclave is placed into an oven at an elevated temperature (typically 200 °C) and kept there for several hours (ESI†). The corresponding autogenous pressure at 200 °C is approx. 17 bar.

Three principal phases can be distinguished in the reaction vessel at the end of the HT process: HT-PPPI appears as orange-yellowish powder at the bottom of the glass liner (a-phase, 92–98 wt%), topped with a second HT-PPPI phase as less-dense, brownish powder (b-phase, 2–8 wt%), and an acidic translucent aqueous phase (c-phase, pH ≈ 1–2). The c-phase is of a reddish hue, which is due to oligomeric oxidation products of PDA (see ESI† for 1H NMR and photographs). The acidic pH is due to PMA, which is present in excess upon the consumption of a certain amount of PDA in its auto-oligomerization. FT-IR-ATR analysis of the dried powders retrieved from phases a and b shows the classical cyclic imide modes ($\tilde{\nu}_{as,C\ O} = 1775\ cm^{-1}$, $\tilde{\nu}_{s,C\ O} = 1720\ cm^{-1}$, and $\tilde{\nu}_{s,C-N} = 1365\ cm^{-1}$) and thus confirms the formation of polyimide (ESI†). Traces of unreacted monomer salt could be detected at reaction times $t_R < 1$ h (ESI†). The lack of amide modes allows us to exclude both crosslinking and the presence of PAAs in the product. HT-PPPI a- and b-phases were insoluble in a variety of solvents (see ESI†). Thermogravimetric analysis reveals high thermal stability ($T_d = 600$ °C, ESI†), which suggests that the product has a high degree of condensation and very few defects.

In order to investigate the crystal growth process and rationalize the micro-morphology of HT-PPPI, scanning electron microscopy (SEM) was performed. Fig. 1A–D show SEM images of the b-phases obtained after HT synthesis at different reaction times. In all samples, microflowers of loosely interstacked petals are visible. Interestingly, these flower-like aggregates depict a striking resemblance to semi-spherical rosette formations of inorganic minerals such as the barite desert rose. Individual petals have a thickness of approx. 100 nm and are several μm wide, while the microflowers are 5–10 μm in diameter. In addition to these flowers, much larger, isolated sheets can be observed. These large sheets have – like the petals – a thickness of approx. 100 nm but are often more than 50 μm wide (compare Fig. 1A and D). As the reaction progresses, new microflower-crystallites nucleate on these sheets, as can be seen in the bottom right corner of Fig. 1A. The SEM micrographs of a-phases obtained at different reaction times are depicted in Fig. 1E–H. In all cases, crystallites are built up of densely packed platelets. Note that these platelets are approx. 1 μm in length, and thus considerably smaller than both the microflower petals and the larger sheets in the b-phase. Again, these smaller platelets seem to grow on previously formed microflowers and larger sheets which act as heterogeneous nuclei for freshly formed HT-PPPI. It is noteworthy that for very short reaction times (1 h and 3 h) we observe hollow particles covered with small crystallites (see centers of Fig. 1E and F) which replicate the rhombohedral shape of the monomer salt crystallites (Fig. 1I and J). This morphological similarity disappears over the course of the reaction. From the morphological evolution, we derive the following crystal growth mechanism (Scheme 2). In the first step, a small amount of the monomer salt is dissolved. In the second step, HT-PPPI is formed by polymerization in solution. HT-PPPI then crystallizes in the third step from these nuclei and forms large sheets and microflowers. Microflowers are semi-spherical aggregates of plate-like crystallites and result from a geometrical selection process (Scheme 2B).[18] Crystallites oriented perpendicularly to the sheet grow faster than crystallites that extend parallel to the sheet. The reason for this is that the concentration of available monomers in close proximity to the sheet has already been lowered, whereas further away the concentration is still high. Thus, crystallites

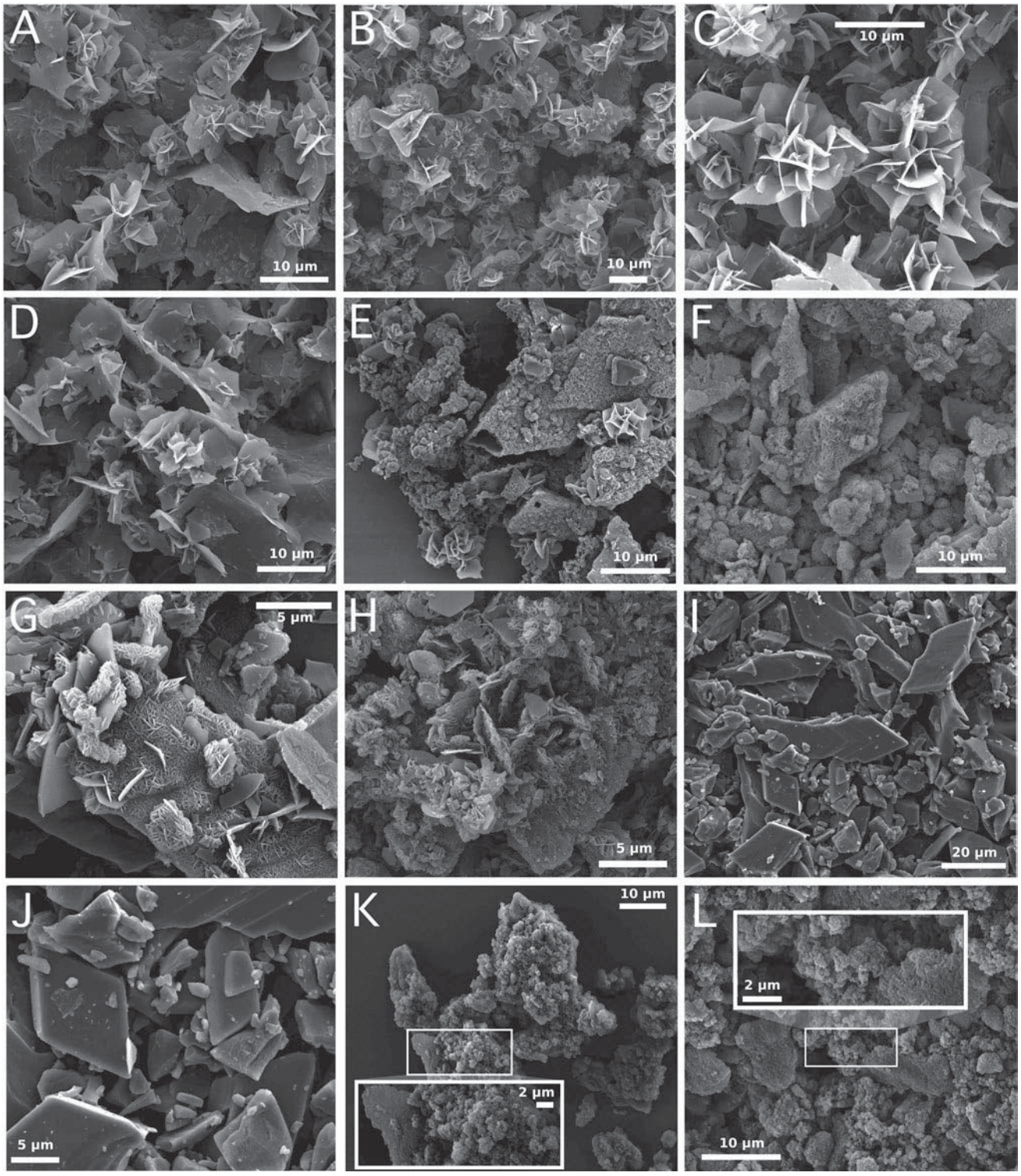

Fig. 1 SEM micrographs of monomer salt and PPPI. (A D) PPPI b-phases of t_R 1 h (A), 3 h (B), 8 h (C), and 12 h (D); (E G) PPPI a-phases of t_R 1 h (E), 3 h (F), 8 h (G) and 12 h (H); (I and J) monomer salt **3**: rhomboid-derived polycrystallites of broad size-distribution; (K) PPPI synthesized in *m*-cresol *via* PAAs and quenched after reaction for comparison; (L) PPPI synthesized in *m*-cresol *via* PAAs and allowed to slowly cool down after reaction for comparison.

growing perpendicular to the sheet are ideally aligned for mass transfer with the reaction mixture.[19] In addition to nascent HT-PPPI sheets, the surface of the monomer salt acts as a site for nucleation. Repeated, rapid crystallization of HT-PPPI near the surface of the monomer salt followed by successive dissolution of the monomer salt leads ultimately to hollow rhombohedral particles, which are covered with small HT-PPPI crystals and replicate the external shape of the original

monomer salt block. HT-PPPI formed in the later stages of the reaction uses microflower petals and large sheets of previously formed PPPI as heterogeneous nuclei, and thus fills the spaces between the observed aggregates. Due to this space filling, the aggregates formed at later stages are much more densely packed than the bare microflowers and large sheets of the early stages of the reaction, and thus sink to the bottom of the autoclave: they become the a-phase. After more than 5 h, the hollow replicas of the original monomer salt fracture, leaving no morphological resemblance between HT-PPPI and starting material. Monomer salts are able to undergo solid-state polymerization to the final PI.[20] This possibility cannot be fully excluded to occur when the crystallites of **3** are surrounded by hydrothermal water. However, the polymerization of monomer salts in the solid-state leads to exact copies of the salt crystallites. As both a- and b-phases do not show such exact, dense copies, but are morphologically quite different, we believe this potential pathway to be highly unlikely in the present case.

The observed morphologies give rise to a major question: is the observed platelet and microflower morphology an intrinsic feature of chemical bonding in PPPI or is it a consequence of the HT process and reaction conditions? In order to clarify the influence of HT conditions on the crystal morphology, we synthesized PPPI classically (*cf.* Scheme 1A), *i.e. via* the corresponding PAAs, in analogy to a previous report (for experimental details, see ESI†).[21] The PPPI dispersion obtained from the classical two-step procedure was separated into two fractions: one part was rapidly precipitated into cold methanol, whereas the other part was allowed to slowly cool down to room temperature, thereby potentially allowing for higher crystallinity.[22] In both cases, FT-IR-ATR confirmed the formation of PPPI (ESI†). However, SEM analysis revealed a striking difference from HT-PPPI: No platelet-like crystallites were observed, but spherical aggregates of roundish particles and fibers (Fig. 1K and L). Subsequently, we subjected the classically synthesized PPPI to HT conditions (200 °C, 12 h) in order to determine whether the obtained morphology could be due to a hydrothermal recrystallization process. SEM analysis shows that the morphology of classically synthesized PPPI remains unchanged by HT treatment (ESI†). This result is a strong indication that the platelet-like morphology of HT-PPPI is a consequence of the hydrothermal polymerization. Moreover, the fact that a classically prefabricated PPPI could not be recrystallized hydrothermally strongly indicates that (i) PPPI molecules do not dissolve hydrothermally, but must simultaneously polymerize and crystallize for obtaining such morphologies, and (ii) it is indeed the monomer salt which dissolves and polymerizes.

In order to verify the degree of crystallinity, we carried out powder X-ray diffraction (PXRD) experiments on dried PPPI and HT-PPPI powders. As evident from Fig. 2A, neither PPPI nor HT-PPPI show reflexions attributed to unreacted monomer salt. Note that classically synthesized PPPI shows some degree of order with two broad amorphous halos centered around 19.5° (2θ) and 27.3–29.0° (2θ), whereas the hydrothermally synthesized a- and b-phases of HT-PPPI are highly crystalline. Indexing of the diffraction patterns for the a- and b-phases of HT-PPPI gives an orthorhombic unit cell with $a = 5.390$ Å, $b = 8.341$ Å, and $c = 12.365$ Å. All principal ($00l$)-reflexes for this unit cell are observed in the PXRD patterns of HT-PPPI (both phases) and the classically prepared PPPI (Fig. 2A). This nicely illustrates the effect of the molecular stiffness of the repeating unit in HT- and classical PPPI, *i.e.* the tecton. This 12.365 Å repeat corresponds to the strut length of PPPI as seen in Fig. 3B, hence we confirm that the principal polyimide chain has been formed *via* both synthesis methods. Fig. 2B shows the diffractograms of the a-phases of hydrothermally synthesized PPPI for various reaction times. Diffractograms of HT-PPPI obtained at $t_R < 1$ h still show several peaks from unreacted monomer salt. Remarkably, the HT polycondensation and crystallization of PPPI at 200 °C appears to be complete after only 1 h, as we see

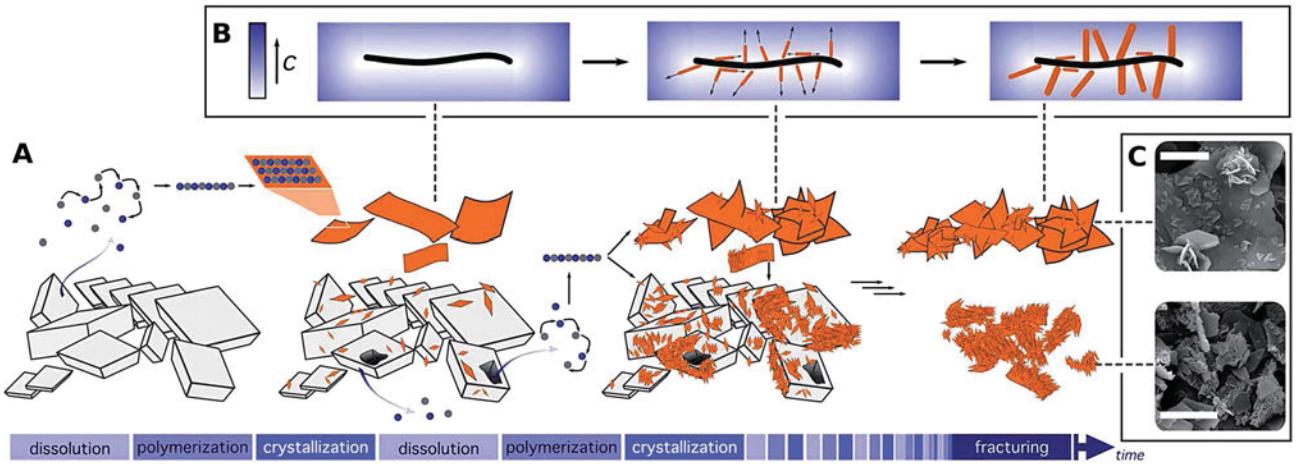

Scheme 2 Hypothesis of HT formation of PPPI. (A) Polycrystalline monomer salt dissolves partially, the comonomers polymerize and as formed PPPI crystallizes; (B) formation of hemispherical polycrystalline "microflower" aggregates by geometrical selection: Nuclei with a perpendicular orientation to the seed PPPI sheet continue growing, whereas nuclei oriented parallel cease growing. This is due to the monomer concentration increasing to higher distances from the sheet. (C) Representative SEM images of a- and b-phases; the scale bar in both images is 5 μm.

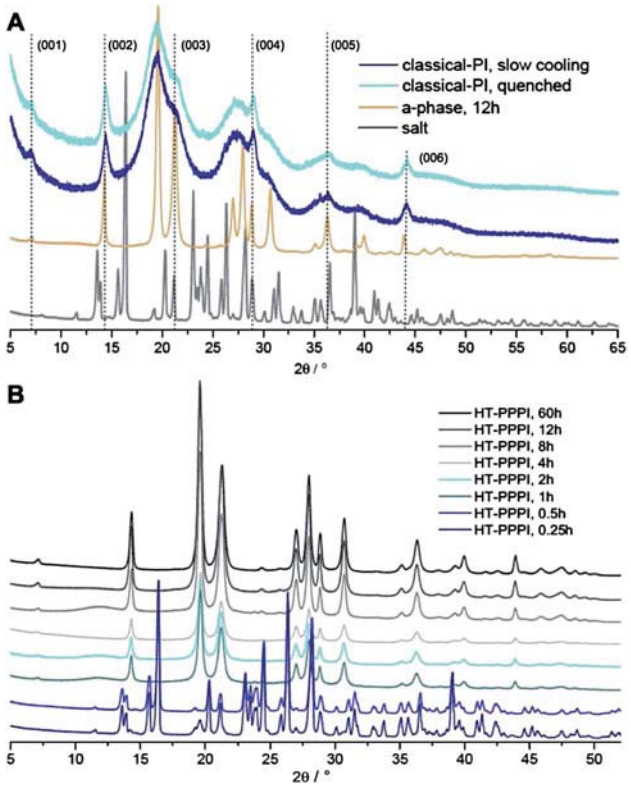

Fig. 2 Diffractograms of PPPI: monomer salt (grey), classically synthesized quenched PPPI (light blue), classically synthesized slowly cooled down PPPI (dark blue), HT synthesized PPPI a-phase (orange), with characteristic (00*l*) Bragg peak positions of HT-PPPI marked as dotted lines (A). Reaction-time dependence of the diffraction data for bulk HT-PPPI synthesized at 200 °C (B).

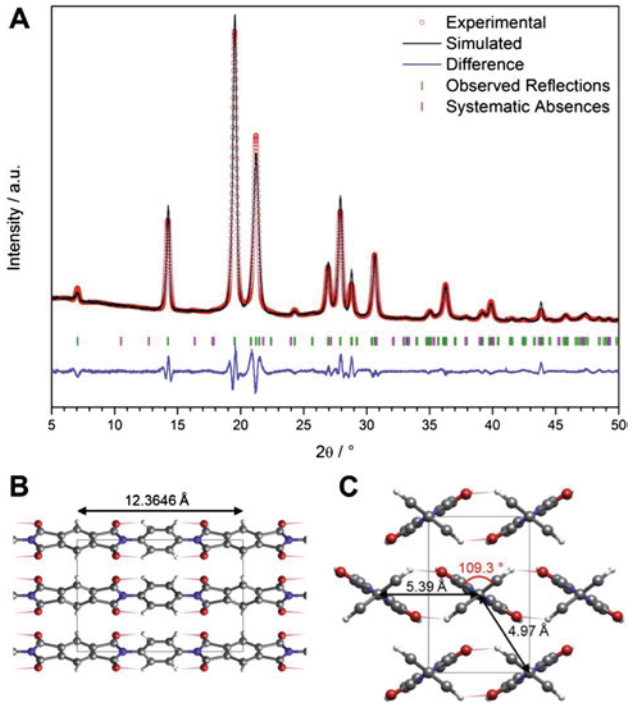

Fig. 3 Rietveld fit performed on the PXRD pattern of HT-PPPI: (R_{wp} 6.70%, R_p 4.60%) with the observed pattern in red, a refined profile in black, a difference plot in blue, and Bragg peak positions in green (observed) and pink (absent) (A). Projection along the *a*-axis (B) and *c*-axis (C) of HT-PPPI with carbon, nitrogen, oxygen and hydrogen atoms represented as grey, blue, red and white spheres, respectively. O H bonds are shown as red-to-white gradient lines (*l*(O H) 2.661 Å, at 132.6°). The parameters of the orthogonal unit cell (*Pbam*, no. 55) are *a* 5.3896 Å, *b* 8.3413 Å, and *c* 12.3646 Å.

no evidence of remaining monomer salt. Even at very long reaction times (t_R = 60 h) we observe no notable change in crystallinity. However, the (*hkl*)- and (*hk*0)-reflexes can only be distinguished in the PXRD profiles of HT-PPPI, while they appear broad and featureless for the classical PPPI. This in turn means that any degree of higher order in between the 1D polyimide chains (*i.e.* along the *a* and *b* axes of the crystallographic unit cell) can only be achieved *via* the HT route.

The PXRD pattern of HT-PPPI (a-phase, prepared at 60 h, 200 °C) is shown in Fig. 3. The *c*-axis of the unit cell coincides with the periodic length along the 1D polyimide chain (12.3646 Å shown in Fig. 3B). This is also the principal repeat which gives rise to the (00*l*) peaks at 7.05, 14.27, 21.51, 28.77, 36.31, and 43.93° (2θ, Cu K_α). Structural refinement suggests that the aryl-linkers are twisted at 109.3° out of the plane of the imide bond. Because of this asymmetric twist, chain-to-chain distances are 5.39 Å along the *a*-axis and 4.97 Å along the *ab*-vector (Fig. 3C). This gives rise to close contacts of 2.661 Å between oxygen and hydrogen atoms of adjacent chains which have been described as weak hydrogen bonds in the literature (Fig. 3C).[23] We attribute the unprecedented crystallinity of HT-PPPI – as seen in the clearly distinguishable (*hk*0) and (*hkl*) reflexes – to the close-packing of chains and the resulting formation of weak O–H bonds.

3 Conclusions

In this contribution we report the hydrothermal synthesis of PPPI, the most rigid, toughest member of the arimid family. The facile, one-step process yields HT-PPPI with outstanding crystallinity and thermal stability (onset of decomposition at 600 °C under N_2). HT-PPPI synthesis was carried out at various reaction times at 200 °C, surprisingly the polymerization and crystallization appears to be complete after only 1 h. FT-IR-ATR, solubility tests and TGA confirm a highly condensed product. The morphology shows microflowers of 5–10 μm in the upper b-phase and densely packed platelets in the major a-phase. A careful analysis of the morphological evolution over time suggests that HT-PPPI crystallites grow *via* a dissolution–polymerization–crystallization process. Moreover, we were able to show that the formation of flower-like morphologies is a consequence of the hydrothermal conditions. The degree of crystallinity is extraordinary: HT-PPPI patterns show no amorphous halos, unlike PPPI obtained *via* established synthesis routes, and enabled an *ab initio* structural refinement. We conclude that the hydrothermal process represents a simple and short route for the synthesis of highly ordered arimids. Compared to conventional polycondensation, this novel route is particularly environmentally friendly as no toxic solvents or

catalysts are required. Given the high temperature stability and remarkable solvent resistance, we believe PPPI to be an interesting candidate for applications under extreme conditions. Intriguingly, HT synthesis of linear PPPI opens up a prospective synthesis strategy towards 2D and 3D polyimides, which have been predicted as fascinating materials in terms of structure, gas storage, and thermal and chemical stability.[24]

Acknowledgements

The authors acknowledge TU Vienna for funding this project. Powder X-ray diffraction measurements were carried out at the X-Ray Center of TU Vienna, and SEM was carried out at the inter-faculty electron microscopy facility of TU Vienna (USTEM). We thank Werner Artner (XRC) for the high-resolution PXRD measurement of HT-PPPI. M. J. B. is holder of a DAAD research fellowship. M. M. U. thanks Jörg Menche, Klaudia Hradil and Ronald Miletich-Pawliczek for fruitful discussion.

References

1 R. J. Young, D. Lu, R. J. Day, W. F. Knoff and H. A. Davis, *J. Mater. Sci.*, 1992, **27**, 5431–5440.
2 D. Bloor, D. J. Ando, F. H. Preston and G. C. Stevens, *Chem. Phys. Lett.*, 1974, **24**, 407–411.
3 O. M. Yaghi, M. O'Keeffe, N. W. Ockwig, H. K. Chae, M. Eddaoudi and J. Kim, *Nature*, 2003, **423**, 705–714.
4 A. P. Cote, A. I. Benin, N. W. Ockwig, M. O'Keeffe, A. J. Matzger and O. M. Yaghi, *Science*, 2005, **310**, 1166–1170.
5 H. M. El-Kaderi, J. R. Hunt, J. L. Mendoza-Cortés, A. P. Côté, R. E. Taylor, M. O'Keeffe and O. M. Yaghi, *Science*, 2007, **316**, 268–272.
6 K. Byrappa and M. Yoshimura, *Handbook of Hydrothermal Technology*, Noyes Publications, 2001.
7 R. A. Laudise, *The Growth of Single Crystals*, Prentice-Hall, 1970.
8 R. A. Laudise and A. A. Ballman, *J. Am. Chem. Soc.*, 1958, **80**, 2655–2657.
9 C. S. Cundy and P. A. Cox, *Chem. Rev.*, 2003, **103**, 663–702.
10 B. Hu, K. Wang, L. Wu, S.-H. Yu, M. Antonietti and M.-M. Titirici, *Adv. Mater.*, 2010, **22**, 813–828.
11 M.-M. Titirici and M. Antonietti, *Chem. Soc. Rev.*, 2010, **39**, 103–116.
12 K. Wakabayashi, T. Uchida, S. Yamazaki and K. Kimura, *Polymer*, 2011, **52**, 837–843.
13 K. Tashiro, *Prog. Polym. Sci.*, 1993, **18**, 377–435.
14 C. E. Carraher Jr and G. Swift, *Functional Condensation Polymers*, Kluwer Academic, 2002.
15 K. Kimura, J.-H. Zhuang, K. Wakabayashi and Y. Yamashita, *Macromolecules*, 2003, **36**, 6292–6294.
16 B. Dao, J. Hodgkin and T. C. Morton, *High Perform. Polym.*, 1999, **11**, 205–218.
17 M. M. Unterlass, D. Kopetzki, M. Antonietti and J. Weber, *Polym. Chem.*, 2011, **2**, 1744–1753.
18 I. Sunagawa, *Crystals: growth, morphology and perfection*, Cambridge University Press, 2005.
19 C. A. Self and C. A. Hill, *J. Cave Karst Stud.*, 2003, **65**, 130–151.
20 M. M. Unterlass, F. Emmerling, M. Antonietti and J. Weber, *Chem. Commun.*, 2014, **50**, 430–432.
21 N. Ritter, I. Senkovska, S. Kaskel and J. Weber, *Macromolecules*, 2011, **44**, 2025–2033.
22 L. Mandelkern, *Crystallization of polymers*, McGraw-Hill, New York, 1964, vol. 1.
23 E. Demers, T. Maris and J. D. Wuest, *Cryst. Growth Des.*, 2005, **5**, 1227–1235.
24 A. Trewin, *CrystEngComm*, 2010, **12**, 2315–2317.